Monthly Notices
of the
ROYAL ASTRONOMICAL SOCIETY

Mon. Not. R. Astron. Soc. **420,** 2715–2726 (2012) doi:10.1111/j.1365-2966.2011.20245.x

Galaxy group around giant radio galaxy NGC 315

R. Chen,[1,2⋆] B. Peng,[1,2,3] R. G. Strom[1,4,5,6] and J. Wei[1]

[1]*National Astronomical Observatories, Chinese Academy of Sciences, Beijing 100012, China*
[2]*Key Laboratory of Radio Astronomy, Chinese Academy of Sciences, Beijing 100012, China*
[3]*Joint Laboratory for Radio Astronomy Technology, Datun Road A20, Beijing 100012, China*
[4]*Netherlands Institute for Radio Astronomy (ASTRON), Postbus 2, 7990 AA Dwingeloo, the Netherlands*
[5]*Astronomical Institute 'Anton Pannekoek', Faculty of Science, University of Amsterdam, the Netherlands*
[6]*Centre for Astronomy, James Cook University, Townsville, QLD 4811, Australia*

Accepted 2011 November 21. Received 2011 November 15; in original form 2011 October 21

ABSTRACT

We have investigated the environment of the giant radio galaxy NGC 315 with its associated group of galaxies selected by their spectroscopic redshifts. Observations were made with the 2.16-m optical telescope at Xinglong Station of the National Astronomical Observatories of China. In addition to 25 galaxies near NGC 315 with published redshifts, we have successfully determined 21 new redshifts of candidates, five of which are previously unknown members of the NGC 315 galaxy group. We examine and discuss the spatial structure and kinematics of this group (which is part of the Perseus–Pisces filament). Nearly 40 per cent of its members are concentrated near NGC 315, close to the emission from its brighter radio jet. The X-ray luminosity implied by the optical velocity dispersion is higher than that derived empirically from observations of other groups, suggesting that X-ray-emitting gas within the NGC 315 group has a low density. This may be one reason for the size of the radio source.

Key words: techniques: spectroscopic – ISM: jets and outflows – galaxies: active – galaxies: distances and redshifts – galaxies: individual: NGC 315 – galaxies: ISM.

1 INTRODUCTION

Giant radio galaxies (GRGs) with linear size larger than 1 Mpc ($H_0 = 75\,\mathrm{km\,s^{-1}\,Mpc^{-1}}$) are the largest celestial objects (Klein et al. 1994). Many GRGs have been found and well studied since their discovery in 1974 (Willis, Strom & Wilson 1974). It is generally believed that the lobes of GRGs move outwards through the low-density (10^{-5} to $10^{-6}\,\mathrm{cm^{-3}}$) intergalactic medium (IGM), and their spectral ages are estimated to be 10^7–10^8 years.

The Fanaroff–Riley type I (FR I) (Fanaroff & Riley 1974) radio galaxy NGC 315 with an unusual Z-shaped structure (see Fig. 5) was first mapped in substantial detail by Bridle et al. (1976), and its extended radio structure was studied further by Bridle et al. (1979), Fomalont et al. (1980), Willis et al. (1981), Jägers (1987), Venturi et al. (1993), Mack et al. (1997), Mack et al. (1998) and Laing et al. (2006). The radio source extending over about 1° is associated with a giant elliptical galaxy at a redshift of 0.016 48 (Trager et al. 2000), which corresponds to a projected linear size of about 1.1 Mpc.

The main jet is quite smooth, elongated along PA = −45° and bends sharply to the south after 18 arcmin (some 340 kpc), while the faint counterjet is directed towards a more diffuse lobe. This intermediate-luminosity FR I source has a radio power of about $\log P_{1.4\,\mathrm{GHz}} = 25.40\,\mathrm{W\,Hz^{-1}}$ (Morganti et al. 2009). On very long baseline interferometry (VLBI) scales, the source also shows clear asymmetry with a bright main jet and a short diffuse counterjet (Venturi et al. 1993). A multi-epoch study of the parsec-scale jet shows evidence for moving features, indicating a mildly relativistic flow (Cotton et al. 1999). X-ray emission associated with NGC 315 has been imaged by *ROSAT* and *Chandra* (Worrall & Birkinshaw 2000; Worrall, Birkinshaw & Hardcastle 2003).

Galaxies around GRGs have been previously studied to examine the influence of the surrounding IGM on the evolution of the radio morphology. DA 240 was investigated by Peng et al. (2004) and Chen et al. (2011b), Chen et al. (2011a) carried out a study of NGC 6251, Subrahmanyan et al. (2008) made observations of MSH 05−22, while MRC B0319−454 was the object of an investigation by Safouris et al. (2009). Compared with FR II galaxies, the FR I radio galaxies are frequently associated with cluster environments (Miller et al. 1999). There is indeed a galaxy group of some 13 members around NGC 315 (Miller et al. 2002). In order to search for more candidates and investigate the nature of galaxies around NGC 315, we have obtained spectra of objects (brighter than 16 mag) within a 40 arcmin radius with the 2.16-m optical telescope at Xinglong Station of National Astronomical Observatories of China (NAOC). The Westerbork Synthesis Radio Telescope (WSRT) observations of NGC 315 at a wavelength of 92 cm have been remapped to compare with the optical galaxies.

The paper is organized as follows. The observations and data reduction appear in Section 2, the results and discussion in Section 3 and the conclusions in Section 4. Throughout, we adopt a flat

⋆E-mail: chenrr@nao.cas.cn

cosmology with $\Omega_m = 0.27$, $\Omega_\Lambda = 0.73$ and a Hubble constant $H_0 = 75\,km\,s^{-1}\,Mpc^{-1}$.

2 OBSERVATIONS AND DATA REDUCTION

2.1 Sample selection

From the NED,[1] we searched for galaxies within a radius of about 40 arcmin (set by the linear size and available observing time) from the NGC 315 nucleus, and find 35 candidates of unknown redshift brighter than ∼16 mag in the *R* band and another 20 galaxies with known redshift from the literature, which are the first 55 listed in Table 1. They are numbered in order of right ascension (RA). Five additional galaxies are considered to be members of the NGC 315 group (Miller et al. 2002); though they lie just outside of the defined search area, they have been added to the end of Table 1 (nos 56–60). After the source number (column 1) there follow the source coordinates (RA and Dec. for J2000 epoch), apparent *R*-band magnitude and redshift (z) with reference if known, in columns 2–5, respectively. The radio source host (NGC 315) entry is italicized.

Apparent *R* magnitudes were taken from the USNO-A 2.0 catalogue. However, nos 33 and 34 are not found in the USNO catalogue so their magnitudes are not listed. Moreover, *R* values for the brightest galaxies in this catalogue are unreliable, so for galaxies with $R < 12$ we have used *B*-, *V*- or *J*-band photometry to estimate *R* (these values are enclosed in brackets). The photometric data come from De Vaucouleurs et al. (1995), the 2MASS survey and Zwicky & Kowal (1968). Magnitudes have been converted to the *R* band using average galaxy colours for spirals ($B - R = 1.26$ and $V - R = 0.52$) and ellipticals ($B - R = 1.56$, $V - R = 0.58$ and $R - J = 1$) (Buta & Williams 1995). We have attempted to include all candidates of $m_r \simeq 16$ or brighter (a limit set by the sensitivity of our instrument), based upon published information, and have also inspected the digital Palomar Observatory Sky Survey (POSS) for missing galaxies.

2.2 Observations

In order to determine redshifts of the selected candidates, spectroscopic observations were performed with the 2.16-m optical telescope and Optomechanics Research (OMR) spectrograph of Xinglong Station, NAOC, using a Tektronix 1024 × 1024 CCD as detector in 2004 August and September, and using a SPEC10 1340 × 400 CCD as detector in 2009 October and 2011 January. We used a 300 $g\,mm^{-1}$ grism and 2.5 arcsec wide slit to get a wavelength coverage of 3800–8000 Å with an average spectral resolution of 4.8 Å. Exposures of 1200–3600 s were taken on the four nights of 2004 August 17 and September 7–9, the nights of 2009 October 17 and 19 and the four nights of 2011 January 28–31. We used helium and argon lamps for the wavelength calibration. The flux calibration was provided by exposures of Kitt Peak National Observatory (KPNO) standard stars (Massey et al. 1988), such as Feige34, HD19445, etc. The atmospheric extinction was corrected for the mean extinction of Xinglong Station, and the telluric O_2 absorption bands at 6870 and 7620 Å were not removed.

2.3 Data reduction

The spectral data were reduced with IRAF[2] software. After the wavelength and flux calibration, each spectrum was inspected for emis-

[1] NASA/IPAC Extragalactic Database.
[2] Image Reduction and Analysis Facility.

Table 1. 35 selected candidate galaxies with magnitude brighter than 16 mag in the *R* band, and another 25 galaxies with published redshift z. For bright galaxies, *R* has been estimated from photometry in other bands (see text).

No.	RA (J2000) (h m s)	Dec. (J2000) (° ′ ″)	*R* app. mag	Redshift z
1	00 55 16.2	30 12 52	15.9	
2	00 55 17.9	30 36 23	15.8	
3	00 55 22.7	30 29 14	(14.5)	0.017 175[a]
4	00 55 32.7	30 23 53	13.1	0.022 105[a]
5	00 55 42.9	30 31 15	14.6	0.022 556[b]
6	00 55 48.5	30 24 31	15.4	
7	00 56 02.3	30 01 13	15.8	
8	00 56 09.3	30 02 29	15.5	
9	00 56 18.8	30 35 29	15.1	
10	00 56 21.6	30 01 48	15.5	
11	00 56 34.3	30 53 31	(14.4)	0.015 801[c]
12	00 56 38.2	30 09 47	14.8	
13	00 56 42.0	30 27 13	17.4	0.016 702[d]
14	00 56 44.7	30 01 31	15.6	
15	00 56 46.8	30 08 25	15.5	
16	00 56 56.9	30 42 50	11.6	
17	00 56 59.0	30 27 15	18.1	0.017 499[d]
18	00 57 00.2	30 38 31	15.9	
19	00 57 00.6	29 45 34	15.6	
20	00 57 01.8	30 29 00	12.5	0.021 965[b]
21	00 57 18.0	30 31 41	15.0	
22	00 57 20.7	30 08 57	15.6	
23	00 57 31.2	30 16 40	15.8	
24	00 57 31.5	30 11 10	13.3	0.016 305[d]
25	00 57 32.1	30 30 16	14.9	0.018 900[b]
26	00 57 32.2	29 46 52	14.2	
27	00 57 32.7	30 16 51	(12.1)	0.016 895[e]
28	*00 57 48.9*	*30 21 09*	*(10.4)*	*0.016 48*[f]
29	00 57 55.0	30 24 32	18.0	0.014 036[d]
30	00 58 01.3	30 42 18	(14.2)	0.015 754[e]
31	00 58 05.2	30 38 57	13.1	
32	00 58 05.2	30 25 32	(13.7)	0.017 702[e]
33	00 58 10.3	30 27 29	-	0.3[g]
34	00 58 10.7	30 27 33	-	0.4[g]
35	00 58 15.4	29 45 42	14.7	
36	00 58 19.0	30 16 05	19.1	0.017 612[d]
37	00 58 20.4	30 09 16	14.8	
38	00 58 21.4	29 53 27	15.1	0.080 700[h]
39	00 58 34.2	30 54 25	12.5	
40	00 58 40.6	30 02 57	14.4	
41	00 58 43.6	29 44 05	15.8	
42	00 58 47.4	29 48 46	14.4	
43	00 58 50.4	30 19 01	14.7	
44	00 58 52.8	29 57 24	15.1	
45	00 59 02.9	30 57 36	15.9	
46	00 59 09.2	30 05 12	(13.4)	
47	00 59 14.5	30 19 22	15.3	
48	00 59 32.2	30 09 12	15.8	
49	00 59 37.9	30 08 03	(14.2)	
50	00 59 44.0	30 51 21	15.2	
51	00 59 59.5	30 34 13	15.9	
52	01 00 29.7	30 34 57	15.6	
53	01 00 33.8	30 06 35	12.2	
54	01 00 38.5	30 18 59	12.1	0.017 299[i]
55	01 00 39.7	30 07 29	(13.7)	0.022 532[a]
56	00 54 59	30 48 20	13.3	0.015 624[b]
57	00 56 09.2	31 04 29	12.4	0.015 564[b]
58	01 00 32.5	30 47 50	(13.2)	0.016 094[b]

Table 1 – *continued*

No.	RA (J2000) (h m s)	Dec. (J2000) (° ′ ″)	*R* app. mag	Redshift *z*
59	01 00 36.5	30 40 07	(11.8)	0.015 938[b]
60	01 01 01.2	29 56 51	14.8	0.016 291[b]

Redshifts are taken from [a]De Vaucouleurs et al. (1995); [b]Miller et al. (2002); [c]Lawrence et al. (1999); [d]Morganti et al. (2009); [e]Huchra, Vogeley & Geller (1999); [f]Trager et al. (2000); [g]Corbin et al. (2000); [h]Keel et al. (2005); [i]Cabanela & Aldering (1998).

sion and/or absorption features. When at least two spectral lines were identified, the average redshift (z) was determined and the error was also estimated. The reduced spectra can be found in Fig. A1, also in order of RA.

The redshifts we obtained from the absorption and/or emission lines are listed in the fifth column of Table 2, while the spectral lines identified are given in the seventh column. We made simple classifications of the objects observed, following the criteria of Veilleux & Osterbrock (1987). Galaxies without emission lines are classified as normal (G), while objects with the Hα emission line but weak forbidden lines of [N II] 6583 Å and [O III] 5007 Å are classified as H II.

The radio data are from observations made with the WSRT at a wavelength of 92 cm. The final cleaned radio map was downloaded from NED, as provided by Mack et al. (1997), and some analysis was done with AIPS[3] software.

3 RESULTS AND DISCUSSION

We observed all 35 selected candidates and successfully determined 21 redshifts that have not been published before. All results are listed in Table 2, in which the first column gives the serial number used in Table 1. Columns 2–8 are the RA+Dec. name, common name, observing date, redshift, exposure time, spectral lines identified and classification of galaxy type [where, for those in the NGC 315 group, early-type (E/S0) and spirals (Sp) are indicated in brackets]. Redshifts taken from the literature are enclosed in brackets, while the redshift column of the 14 candidates whose spectra were too noisy to identify any features have no entry. [Most of them are fainter than 15 mag in the *R* band (Fig. 2).] In addition, no. 23 was found to have zero redshift so it is probably a star (though it could be a star superimposed on a faint galaxy).

Leaving aside the 15 objects with no (or zero) redshift, let us consider the remaining 45 galaxies with redshifts. A histogram of their redshift distribution (Fig. 1, excluding eight objects with $z > 0.1$) shows the greatest concentration at $z \simeq 0.016$. This group of 23 galaxies (including the radio source host, NGC 315) lies in the redshift range between 0.014 and 0.019. These galaxies pass the (3σ) velocity dispersion test suggested by Yahil & Vidal (1977). There is an adjacent peak which consists of four galaxies at $z \simeq 0.022$, which do not pass the 3σ criterion if we add them to the group of 23. We therefore consider them to be a small background group. The next most significant grouping consists of four galaxies at considerably higher redshifts near $z = 0.067$. The NGC 315 group has been studied before (Miller et al. 2002), and the work reported here adds five new members. For three of the five, the spectra show emission lines (they are of H II type, see Table 2).

[3] Astronomical Image Processing System.

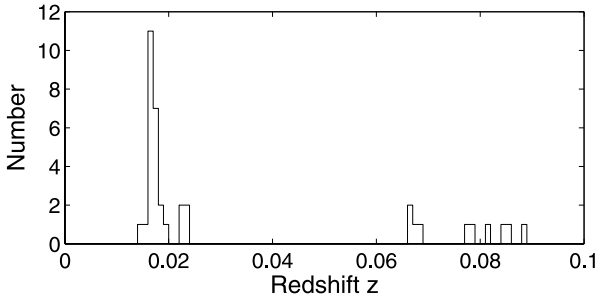

Figure 1. Histogram of the redshift distribution for 37 of the 45 galaxies with $z < 0.1$ from Table 2. The highest peak is due to members of the NGC 315 group.

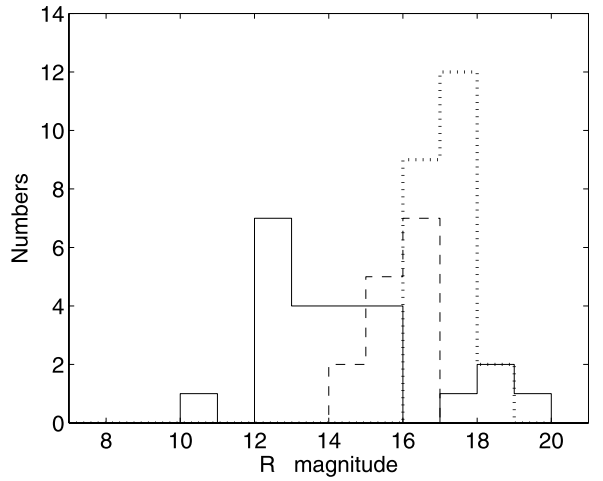

Figure 2. A histogram showing the *R* magnitudes of the group of galaxies we have studied (Table 2) traced with a solid line, while a dashed line shows the magnitudes of the remaining galaxies from Table 2 with low signal-to-noise ratio (S/N) (and hence no reliable redshift). A dotted line gives the magnitudes of the remaining USNO galaxies.

The magnitudes of the 23 galaxies in the NGC 315 group are indicated by a solid line in the histogram of Fig. 2, where the host is the brightest of the group. The cut-off for $m > 16$ is due to the limited sensitivity of the 2.16-m telescope. The galaxies fainter than $m \sim 17$ have redshifts determined by their 21-cm H I emission (Morganti et al. 2009). Magnitudes of the 14 objects with low S/N are indicated by a dashed line, while the unobserved candidates fainter than 16 mag in our search region are marked using a dotted line.

The NGC 315 group is part of an extensive galaxy conglomeration whose large-scale structure has been the subject of a number of previous studies. NGC 315 and its companions lie at the south-western end of a long stretch of galaxies catalogued as Zw 0107.5 +3 212 (Zwicky & Kowal 1968). Fig. 3 shows the distribution of galaxies with $z \simeq 0.016$ in a $10^\circ \times 10^\circ$ region centred on NGC 315. One can clearly see the lane of galaxies stretching off to the north-east, and the fact that there are also members of the grouping, though at a lower density, to the west. The whole complex is part of the Perseus–Pisces filament, with the two concentrations north-east of NGC 315 being centred on their dominant members NGC 383 and NGC 507, as indicated. Histograms (Fig. 4) show that the three small groups have practically identical redshifts. Nolthenius (1993) used an algorithm to determine membership for over 150 groups, including NGC 315 (and NGC 383), and found that four

Table 2. Summary of all results: 35 candidates observed with the 2.16-m optical telescope and 25 additional ones from other sources like NED (observing dates left blank, z enclosed in brackets) including five galaxies outside our search region (nos 56−60).

No.	RA+Dec. name (J2000)	Common name	Obs. dates (yyyy.mm.dd)	Redshift z	Exposure (s)	Notes	C
1	005516+301252		2009.10.17	–	3600	Low S/N	–
2	005517+303623		2011.01.29	–	3600	Low S/N	–
3	005522+302914	CGCG 501−043	–	(0.017 175)	–	–	(Sp)
4	005532+302353	CGCG 501−047	–	(0.022 105)	–	–	–
5	005542+303115		–	(0.022 556)	–	–	–
6	005548+302431		2009.10.19	0.0683±0.0005	3600	Mg*b*, Na D	G
7	005602+300113		2011.01.28	0.0773±0.0001	3600	Hα, [N II]	H II
8	005609+300229		2009.10.19	–	3600	Low S/N	–
9	005618+303529		2009.10.17	–	3600	Low S/N	–
10	005621+300148		2009.10.19	0.1407±0.0004	3600	Hα, [N II], Na D	H II
11	005634+305331	KUG 0053+306	–	(0.015 801)	–	–	(Sp)
12	005638+300947		2009.10.17	–	3600	Low S/N	–
13	005642+302713		–	(0.016 702)	–	–	(Sp)
14	005644+300131		2009.10.19	–	3600	Low S/N	–
15	005646+300825	2MFGC 00684	2004.09.09	–	1800	Low S/N	–
16	005656+304250		2004.09.07	0.0164±0.0006	1200	Mg*b*, Na D, *G* band	G (E?)
17	005659+302715		–	(0.017 499)	–	–	(Sp)
18	005700+303831		2004.09.09	0.0853±0.0012	3600	*G* band, Mg*b*, Fe E, Na D	G
19	005700+294534		2011.01.29	–	3600	Low S/N	–
20	005701+302900	FGC 0110	–	(0.021 965)	–	–	–
21	005718+303141		2004.09.07	0.0844±0.0014	3600	*G* band, Hβ, Mg*b*, Na D	G
22	005720+300857		2004.09.07	0.1257±0.0005	3600	Hβ, Mg*b*, Na D	G
23	005731+301640		2004.09.08	0	3600	*G* band, Mg*b*, Na D	star
24	005731+301110		–	(0.016 305)	–	–	(Sp)
25	005732+303016		–	(0.018 900)	–	–	(E?)
26	005732+294652		2004.09.09	–	3600	Low S/N	–
27	005732+301651	NGC 311	–	(0.016 895)	–	–	(S0)
28	005748+302109	NGC 315	–	(0.016 48)	–	–	(E)
29	005755+302432		–	(0.014 036)	–	–	(Sp)
30	005801+304218	CGCG 501−055	–	(0.015 754)	–	–	(Sp)
31	005805+303857		2004.09.08	0.0659±0.0012	3600	*G* band, Mg*b*, Na D	G
32	005805+302532	NGC 318	–	(0.017 702)	–	–	(E?)
33	005810+302729		–	(0.3)	–	–	–
34	005810+302733		–	(0.4)	–	–	–
35	005815+294542		2009.10.17	–	3600	Low S/N	–
36	005819+301605		–	(0.017 612)	–	–	(Sp)
37	005820+300916		2004.09.08	0.0673±0.0005	3000	*G* band, Mg*b*, Na D	G
38	005821+295327		–	(0.080 700)	–	–	–
39	005834+305425		2004.09.08	0.0155±0.0006	3600	Hα, [N II], [S II]	H II (E)
40	005840+300257		2004.09.09	0.0776±0.0001	3600	Na D, Hα, [N II]	H II
41	005843+294405		2011.01.30	–	3600	Low S/N	–
42	005847+294846		2009.10.17	0.0664±0.0002	3600	Na D, Hα, [N II]	H II
43	005850+301901		2009.10.19	0.1203±0.0002	3600	*G* band, Mg*b*, Na D	G
44	005852+295724		2009.10.19	0.1026±0.0012	3600	Mg*b*, Fe E, Na D	G
45	005902+305736		2011.01.31	0.1195±0.0002	3600	Hα, [N II]	H II
46	005909+300512		2004.08.17	0.0169±0.0014	3000	*G* band, Mg*b*, Na D	G (E?)
47	005915+301922		2009.10.19	0.1206±0.0021	3600	*G* band, Hβ, Mg*b*, Na D	G
48	005932+300910		2011.01.28	0.0885±0.0026	3600	Mg*b*, Na D	G
49	005937+300803		2009.10.17	–	3600	Low S/N	–
50	005944+305121		2009.10.19	0.0167±0.0001	3600	Hα, [N II]	H II (E)
51	005959+303413		2011.01.28	–	3600	Low S/N	–
52	010029+303457	B2 0057+30C	2011.01.29	–	3600	Low S/N	–
53	010033+300635		2009.10.17	0.0161±0.0004	3600	Mg*b*, Fe E, Na D	G (Sp)
54	010038+301859		–	(0.017 299)	–	–	(Sp)
55	010039+300729	CGCG 501−060	–	(0.022 532)	–	–	–
56	005459+304820		–	(0.015 624)	–	–	(Sp?)
57	005609+310429	UGC 575	–	(0.015 564)	–	–	(Sp)
58	010032+304750	IC 66	–	(0.016 094)	–	–	(Sp)
59	010036+304007	NGC 338	–	(0.015 938)	–	–	(Sp)
60	010101+295651	UGC 630	–	(0.016 291)	–	–	(Sp)

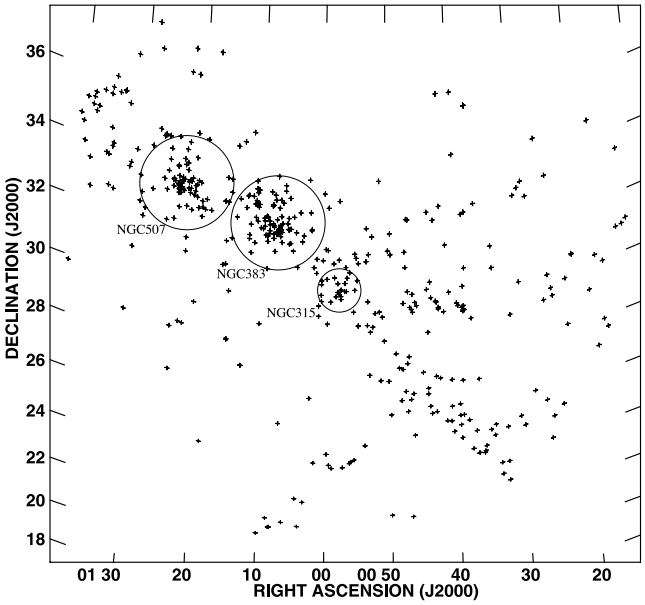

Figure 3. Locations of all galaxies within a radius of 10° from the NGC 315 host and in the redshift range of $0.0140 \leq z \leq 0.0189$. Rough locations of the three groups on the Perseus–Pisces filament are indicated by circles.

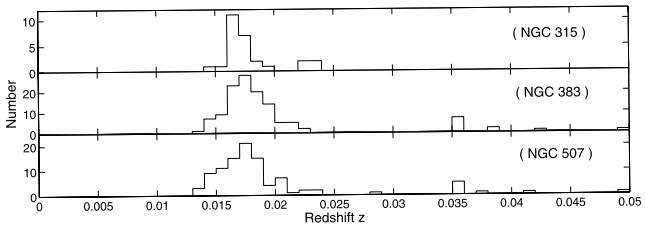

Figure 4. Redshift distribution of three groups associated with NGC 315, NGC 383 and NGC 507.

of the galaxies in his input sample (nos 27, 28, 59 and UGC 598 which lie well north of our search area) belonged to the group. Their dispersion was computed to be 122 km s^{-1}.

Garcia (1993), drawing upon a well-defined sample of over 23 000 galaxies (Garcia et al. 1993), made a study of several hundred groups, including the three mentioned above. Group membership was decided on the basis of several methods, resulting in a set of definite and possible members. In the case of the NGC 315 group, 18 definite members (and another 24 possible) were found, but they are spread over a much larger region than that sampled here: well over half lie outside of our 40 arcmin radius search area. Among the companions of NGC 315 within 20 arcmin, both the Garcia and Nolthenius studies include only NGC 311. The more distant galaxies constitute a section of the 'background' Perseus–Pisces filament. Miller et al. (2002), in a study of groups associated with nearby radio galaxies, found NGC 315 to have a dozen companions. Four of the group members (including NGC 315 itself) lie within 250 kpc of the centre. Miller et al. (2002) further calculated the dispersion of all the galaxies within the group to be 267 km s^{-1}, while for those within 250 kpc it rises to 308 km s^{-1}.

Recently, Morganti et al. (2009) carried out a study of 21-cm H I in NGC 315, examining not only absorption against continuum emission from the galaxy's nuclear region, but also discovering weak emission from an area just south-west of the nucleus. They concluded that this may be gas from a recent accretion event which

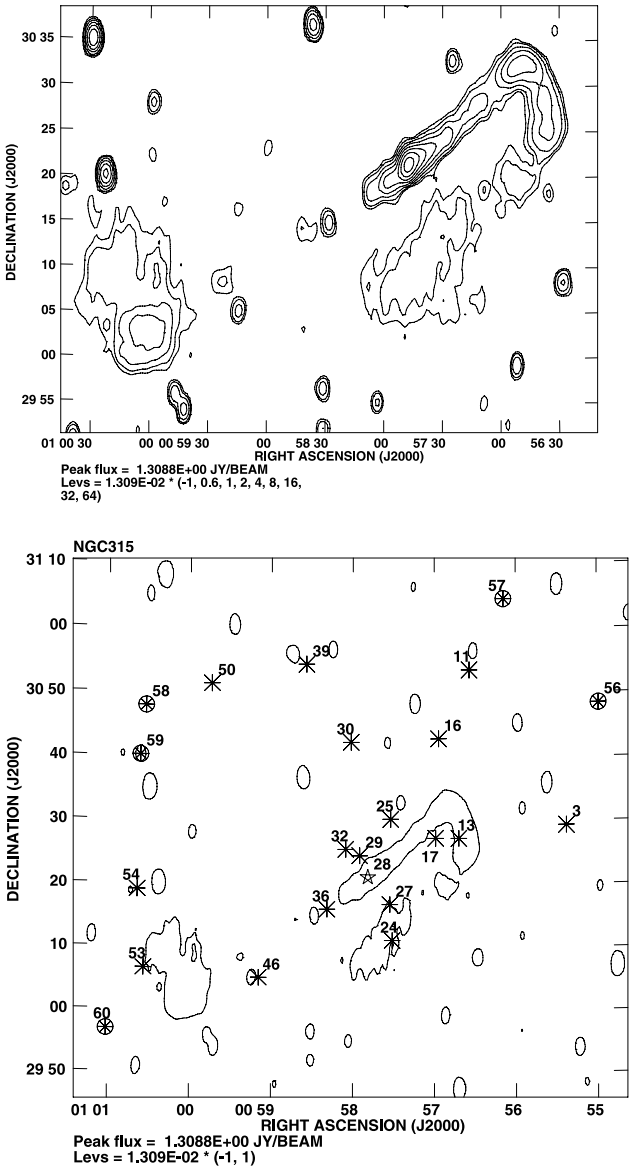

Figure 5. Above: NGC 315 contour map (showing the radio extent) obtained with the WSRT at 92 cm. Below: a single contour map with the 23 optical galaxies at redshifts $0.014 \leq z \leq 0.019$. The galaxies are numbered and members within the search area are plotted with asterisks (except NGC 315, which is indicated by a star), while the five beyond our search radius are shown by asterisks in circles.

could be fuelling the radio source. Their observation has also detected H I emission from five other companion galaxies within the NGC 315 group. In combination with the 13 galaxies (including NGC 315 itself) studied by Miller et al. (2002), this brought the group membership to 18, to which we have now added another five. The locations of the group members are shown in Fig. 5. The detailed radio map of NGC 315 is shown in Fig. 5 (upper), where one can see the main jet emanating from the bright nuclear region stretching nearly 20 arcmin to the north-west before abruptly turning to the south, widening and turning again to end in extended, amorphous emission south of the galaxy. The figure also shows the fainter counterjet which produces two short patches of emission to the south-east, and an extended lobe some 35 arcmin from the

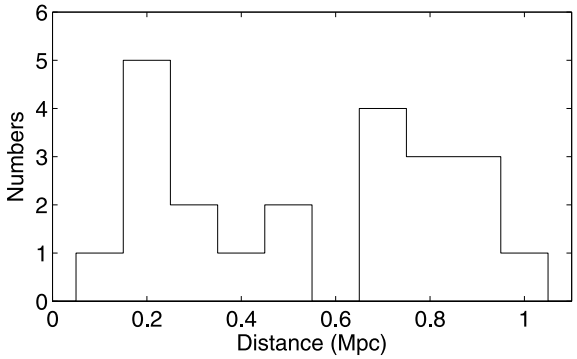

Figure 6. Relative distance distribution of the 22 member galaxies from the GRG host, NGC 315.

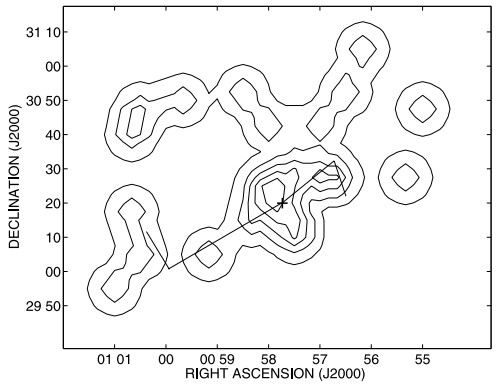

Figure 7. Smoothed distribution of galaxies in the NGC 315 group. The contour levels run from 0.2 to 1.8 (in steps of 0.4) galaxies pixel^{-1} (for a pixel size of 150 × 150 arcsec^2). The location of NGC 315 is indicated by a cross, while four line segments show the ridge line of the jets and main lobes of the radio emission.

nucleus, which turns northwards. The abrupt bends in the jet and counterjet give the radio source its trademark 'inverted-N' shape.

Fig. 5 (lower panel) shows all the galaxies which, on the basis of redshift ($z = 0.0165 \pm 0.0025$), belong to the group associated with NGC 315. The distribution is rather asymmetric, with a compact group around the host galaxy, other members scattered to the north and east, and nothing to the south-west. A histogram showing the distribution with distance from NGC 315 (Fig. 6) clearly illustrates this, with half of the companions located beyond 0.6 Mpc: these are principally the galaxies to the north and east. The compact central group clusters around the main jet, and its dominance is clearly shown by a smoothed map of the galaxy distribution (Fig. 7), suggesting that the inner nine galaxies constitute a subgroup. Although Miller et al. (2002) found no evidence for significant substructure in the group, their sample included only NGC 315 and three of its companions near the radio source. Kinematically, all the galaxies shown in Fig. 5 (lower panel) have a velocity spread of 1460 km s^{-1}, and a dispersion of $\sigma = 291$ km s^{-1}. For the inner cluster around NGC 315, we find $\sigma = 400$ km s^{-1}. The kinematics of the systems is shown graphically in Fig. 8. Since NGC 315 and its close companions are embedded in the Perseus–Pisces filament, and the subgroup is spatially separated to some extent from other galaxies in the filament, it makes sense to consider it as a possible separate entity in the following discussion.

The X-ray emission of NGC 315 consists of a combination of galaxy-scale emission principally from a hot X-ray-emitting atmosphere and unresolved emission which fits a power-law spectrum (Worrall et al. 2003). From a correlation between velocity dispersion and X-ray luminosity (Mulchaey & Zabuldoff 1998), using the velocity dispersion of the whole group (23 galaxies), $\sigma_{r1} = 291$ km s^{-1}, we derive an expected X-ray luminosity of 2.7×10^{42} erg s^{-1}. This value is about one order of magnitude higher than the gas luminosity reported by Worrall et al. (2003), $L_{\rm x} = 3.1 \times 10^{41}$ erg s^{-1} (corrected to the same H_0). If we consider just the nine members around the north-west lobe, the velocity dispersion is $\sigma_{r2} = 400$ km s^{-1}, and the implied X-ray luminosity is 9.9×10^{42} erg s^{-1}, which is well over an order of magnitude higher than observed. Although this result is similar to what we found in the case of the FR II radio galaxy NGC 6251 (Chen et al. 2011a), where the observed value is also much less than expected, it should be noted that the scatter in the correlation found by Mulchaey & Zabuldoff (1998) is considerable.

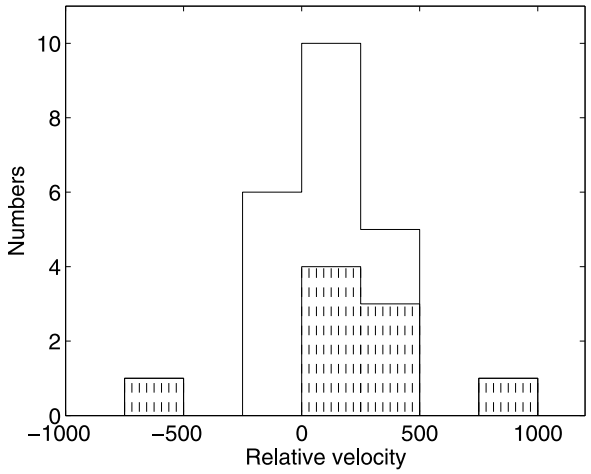

Figure 8. Relative velocity distribution of the 23 members of the NGC 315 group, of which the nine members around the north-west lobe are traced by dashed lines. The zero-point is the systemic velocity of the host galaxy.

The most likely explanation for the lower than expected X-ray luminosity is that the gas density in the extended component is low. However, this may only be the case for the hot component, and there could still be significant cool, neutral gas in the surroundings. Morganti et al. (2009) have suggested as much on the basis of their observations of 21-cm H I emission from both NGC 315 itself, where accretion may be taking place, and from the companion galaxies surrounding it. [We note moreover that another seven galaxies in the group (but farther removed from NGC 315) – nos 3, 30, 56, 57, 58, 59 and 60 – also have H I emission (Giovanelli & Haynes 1985; Huchtmeier & Richter 1989); the group is spiral rich.] In fact, it is most striking that the brighter, shorter radio jet in the source coincides with the region of greatest galaxy density. The contrast between the jet and counterjet in this source is not the result of relativistic effects for, although the jet shows relativistic motion near the nucleus (Cotton et al. 1999), over most of its length it is only mildly relativistic, $v/c \simeq 0.4$ (Canvin et al. 2005). We suggest that the jet has been strongly influenced by its environment as delineated by the compact group of surrounding galaxies. This can be seen in both its physical size and radio brightness when compared with the source's counterjet.

4 CONCLUSIONS

In our continuing research following the study of the GRGs DA 240 and NGC 6251, we have made spectroscopic observations of galaxy

candidates brighter than 16 mag in the *R* band, within 40 arcmin of NGC 315. 20 spectra and redshifts have been determined (after eliminating one likely star) for candidates on our list, and five new members of the NGC 315 group have been identified. Similar to the case of the radio galaxy NGC 6251, the X-ray luminosity expected from the L_x–σ_r relationship for the NGC 315 group is at least an order of magnitude higher than the observed value. This suggests that the density of X-ray-emitting intergroup gas around NGC 315 is quite low, although the 21-cm H I observations (Morganti et al. 2009) may indicate the presence of a significant neutral component.

It is interesting to compare the galaxies around NGC 315 with the groups associated with NGC 6251 and the more distant southern GRGs MSH 05−22 (Subrahmanyan et al. 2008) and MRC B0319−454 (Safouris et al. 2009). NGC 315, NGC 6251 and MRC B0319−454 all have a bright radio jet on one side opposite a longer, fainter counterjet, while in MSH 05−22 the main jet is longer than the counterjet. The four double radio sources have asymmetrical lobes, with length ratios ranging from 1.5 to 2. In MRC B0319−454 and MSH 05−22 the main jet is directed towards the more distant radio lobe, but in the other pair the opposite is the case. All four GRGs are associated with galaxy groups, containing 23 and 17 members in the case of NGC 315 and NGC 6251, and around 50 each for the other two. The small group associated with NGC 6251 is densest near the dominant host galaxy, while the other three lie on the peripheries of larger groups/clusters. In all four a handful of companions forms a subgroup around their GRG hosts.

Subrahmanyan et al. (2008) and Safouris et al. (2009) find evidence that the radio lobes in MSH 05−22 and MRC B0319−454 have been influenced by their environment. In the former source, the shorter lobe, which is also displaced from the radio source major axis, is directed towards the main galaxy concentration of the whole group. Assuming the galaxy and gas densities to be correlated, the relative lobe location can be explained by density gradients, and perhaps buoyancy forces. In the case of MRC B0319−454, Safouris et al. (2009) find that the more distant lobe lies in an underdense part of the group, with its major axis directed laterally to a line joining its hotspot with the host galaxy. These features can also be explained by differences in the ambient density, and plausibly by buoyancy effects. In MRC B0319−454 and NGC 315, the subgroup around the host is concentrated about the shorter, brighter radio component. For NGC 6251 this might be the case (there are fewer galaxies to the south-east of the host, the counterjet side), but in MSH 05−22 it is not so: the subgroup lies between the two radio lobes. There is thus significant evidence that the ambient medium is affecting the radio morphologies of these four sources. To continue our investigation of the environments of GRGs, we are extending this kind of study to other nearby sources.

ACKNOWLEDGMENTS

This work was partially supported by China Ministry of Science and Technology under State Key Development Programme for Basic Research (2012CB821800), the Open Project Programme of the Key Laboratory of Optical Astronomy and the Key Laboratory of Radio Astronomy, NAOC, CAS. The Westerbork Synthesis Radio Telescope is operated by the Netherlands Institute for Radio Astronomy (ASTRON), with financial support from the Netherlands Organization for Scientific Research (NWO). The research of RGS has been supported by a Chinese Academy of Sciences Visiting Professorship for Senior International Scientists, Grant No. 2009J2-1. This research has made use of the NASA/ADS Abstract Service, and of NED which is operated by the Jet Propulsion Laboratory, Caltech, under contract with the National Aeronautics and Space Administration. We are grateful for the use of the USNO-A2.0 catalogue.

REFERENCES

Bridle A. H. et al., 1976, Nat, 262, 179
Bridle A. H. et al., 1979, ApJ, 228, L9
Buta B., Williams K. L., 1995, AJ, 109, 543
Cabanela J. E., Aldering G., 1998, AJ, 116, 1094
Canvin J. R., Laing R. A., Bridle A. H., Cotton W. D., 2005, MNRAS, 363, 1223
Chen R., Peng B., Strom R. G., Wei J., 2011a, MNRAS, 412, 2433
Chen R., Peng B., Strom R. G., Wei J., Zhao Y., 2011b, A&A, 529, A5
Corbin M. R., Vacca W. D., O' Neil E., Thompson R. I., 2000, AJ, 119, 1062
Cotton W. D., et al., 1999, ApJ, 519, 108
De Vaucouleurs G. et al. 1995, VizieR Online Data Catalog, 7155, 0
Fanaroff B. L., Riley J. M., 1974, MNRAS, 167, L31
Fomalont E. B., Bridle A. H., Willis A. G., Perley R. A., 1980, ApJ, 237, 418
Garcia A. M., 1993, A&AS, 100, 47
Garcia A. M., Paturel G., Bottinelli L., Gouguenheim L., 1993, A&AS, 98, 7
Giovanelli R., Haynes M. P., 1985, AJ, 90, 2445
Huchra J. P., Vogeley M. S., Geller M. J., 1999, ApJS, 121, 287
Huchtmeier W. K., Richter O.-G., 1989, A General Catalog of H I Observations of Galaxies. Springer-Verlag, New York
Jägers W. J., 1987, A&AS, 71, 75
Keel W. C. et al., 2005, ApJS, 158, 139
Klein U. et al., 1994, A&A, 283, 729
Laing R. A., Canvin J. R., Cotton W. D., Bridle A. H., 2006, MNRAS, 368, 48
Lawrence A. et al., 1999, MNRAS, 308, 897
Mack K. H., Klein U., O' Dea C. P., Willis A. G., 1997, A&A, 123, 423
Mack K. H. et al., 1998, A&A, 329, 431
Massey P., Strobel K., Barnes J. V., Anderson E., 1988, ApJ, 328, 315
Miller N. A., Owen F. N., Burns J. O., Ledlow M. J., Voges W., 1999, AJ, 118, 1988
Miller N. A., Ledlow M. J., Owen F. N., Hill J. M., 2002, AJ, 123, 3018
Morganti R. et al., 2009, A&A, 505, 559
Mulchaey J. S., Zabludoff A. I., 1998, ApJ, 496, 73
Nolthenius R., 1993, ApJS, 85, 1
Peng B., Strom R. G., Wei J., Zhao Y. H., 2004, A&A, 415, 487
Safouris V., Subrahmanyan R., Bicknell G. V., Saripalli L., 2009, MNRAS, 393, 2
Subrahmanyan R., Saripalli L., Safouris V., Hunstead R. W., 2008, ApJ, 677, 63
Trager S. C., Faber S. M., Worthey G., González J. J., 2000, AJ, 119, 1645
Veilleux S., Osterbrock D. E., 1987, ApJS, 63, 295
Venturi T. et al., 1993, ApJ, 408, 81
Willis A. G., Strom R. G., Wilson A. S., 1974, Nat, 250, 625
Willis A. G., Strom R. G., Bridle A. H., Fomalont E. B., 1981, A&A, 95, 250
Worrall D. M., Birkinshaw M., 2000, ApJ, 530, 719
Worrall D. M., Birkinshaw M., Hardcastle M. J., 2003, MNRAS, 343, L73
Yahil A., Vidal N. V., 1977, ApJ, 214, 347
Zwicky F., Kowal C. T., 1968, Catalog of Galaxies and of Clusters of Galaxies, Vol. VI. California Institute of Technology, Pasadena

APPENDIX A

Spectra of the 35 galaxies around NGC 315, observed with the 2.16-m optical telescope at Xinglong Station of the NAOC.

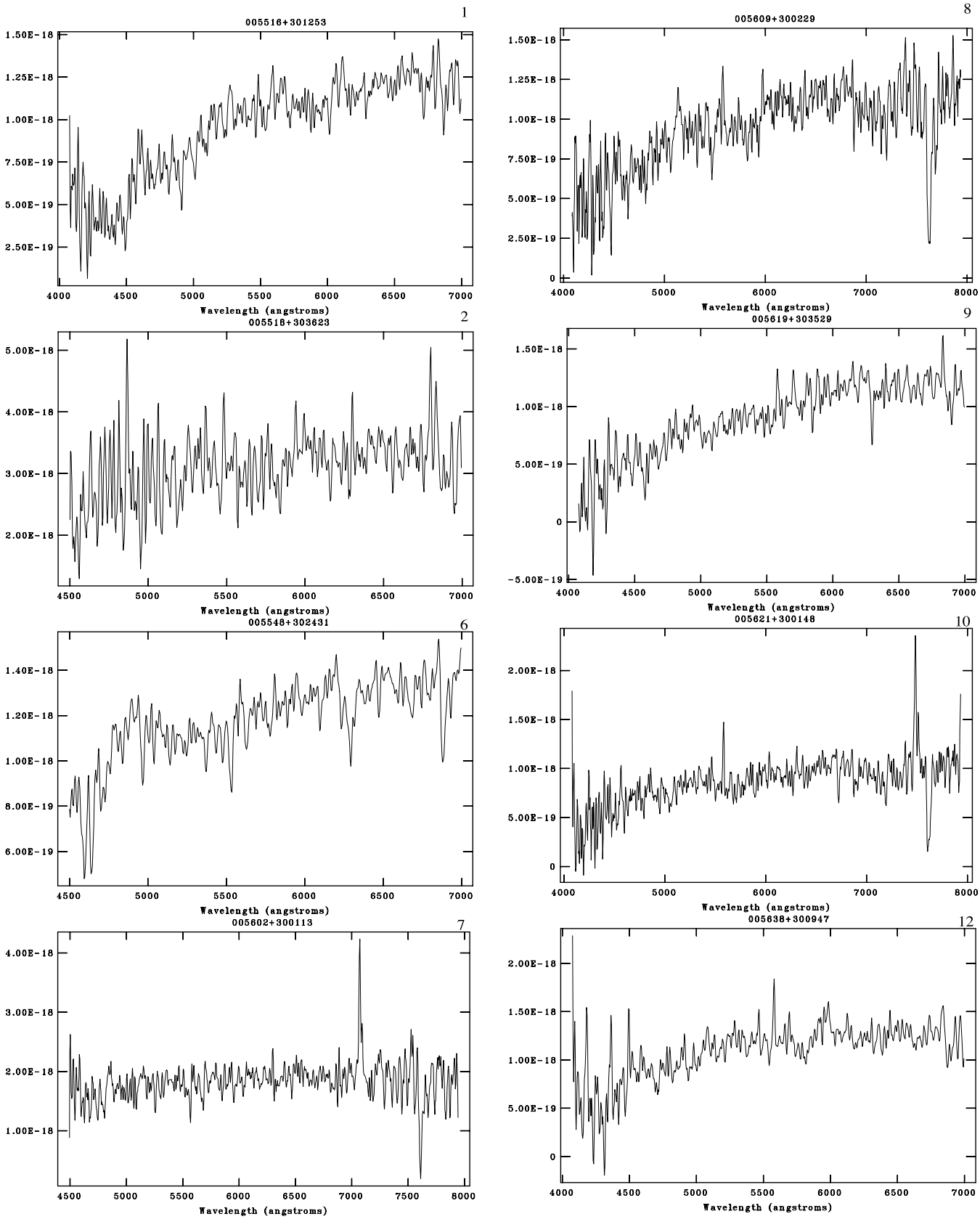

Figure A1. Spectra of the 35 galaxies around NGC 315, observed with the 2.16-m optical telescope at Xinglong Station of the NAOC.

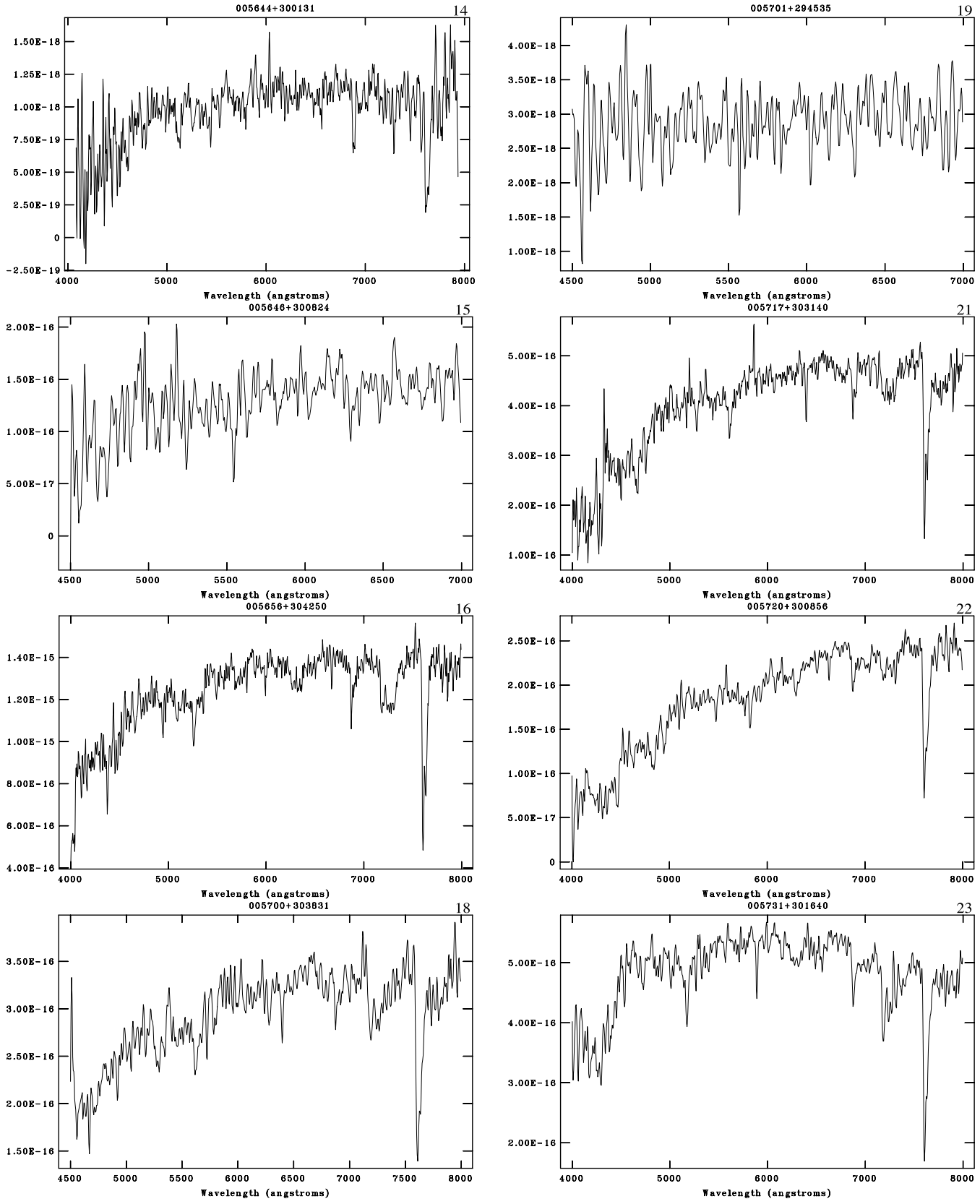

Figure A1 – *continued*

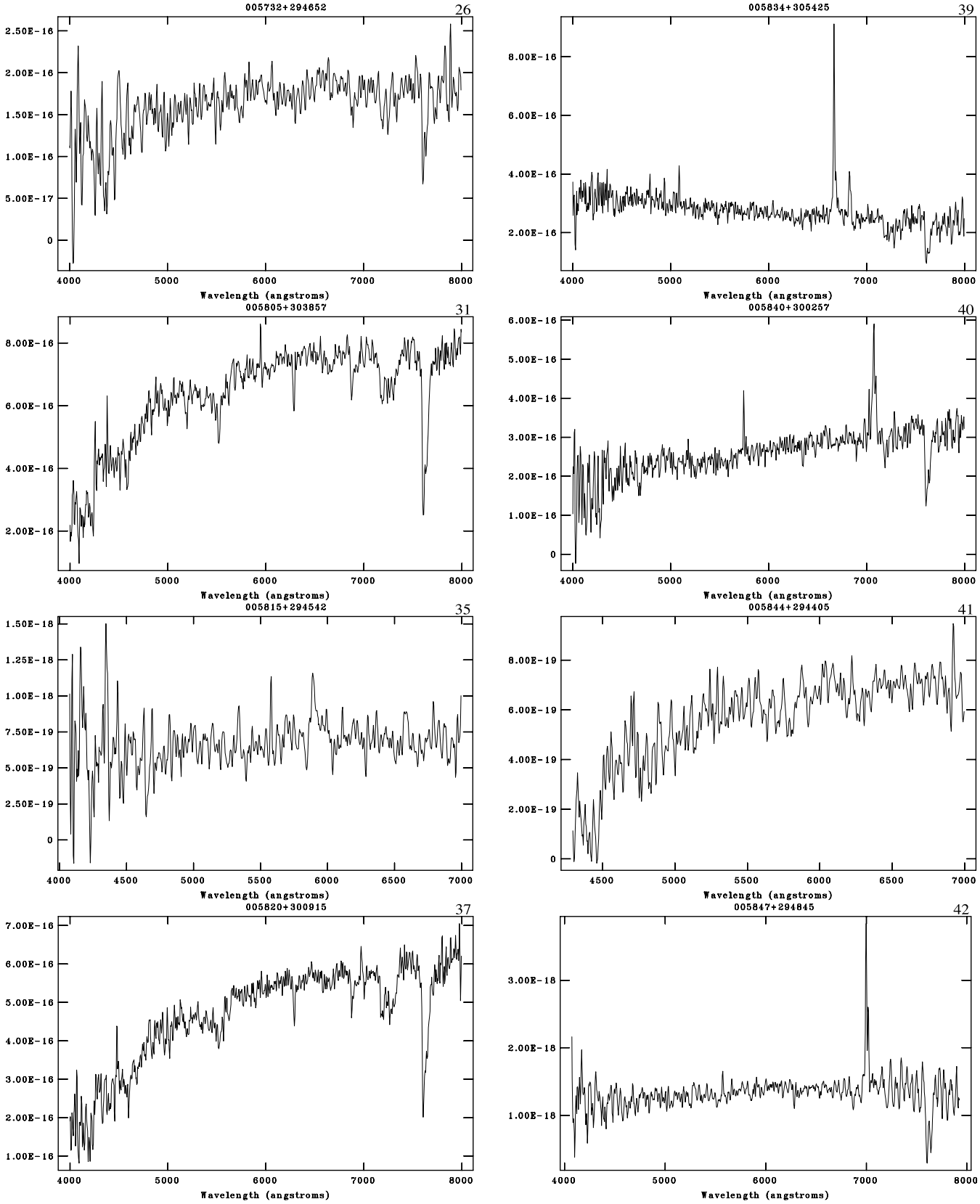

Figure A1 – *continued*

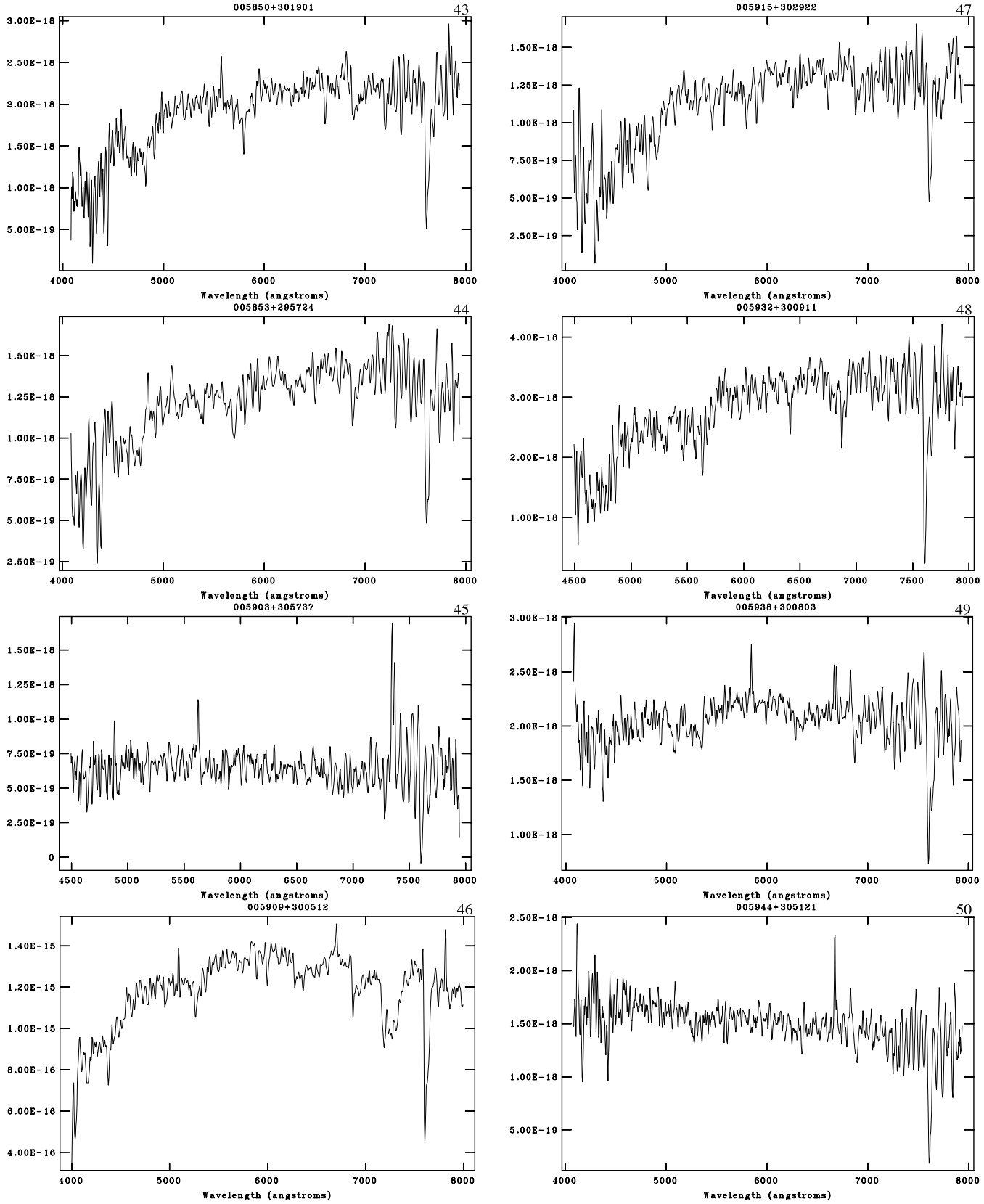

Figure A1 – *continued*

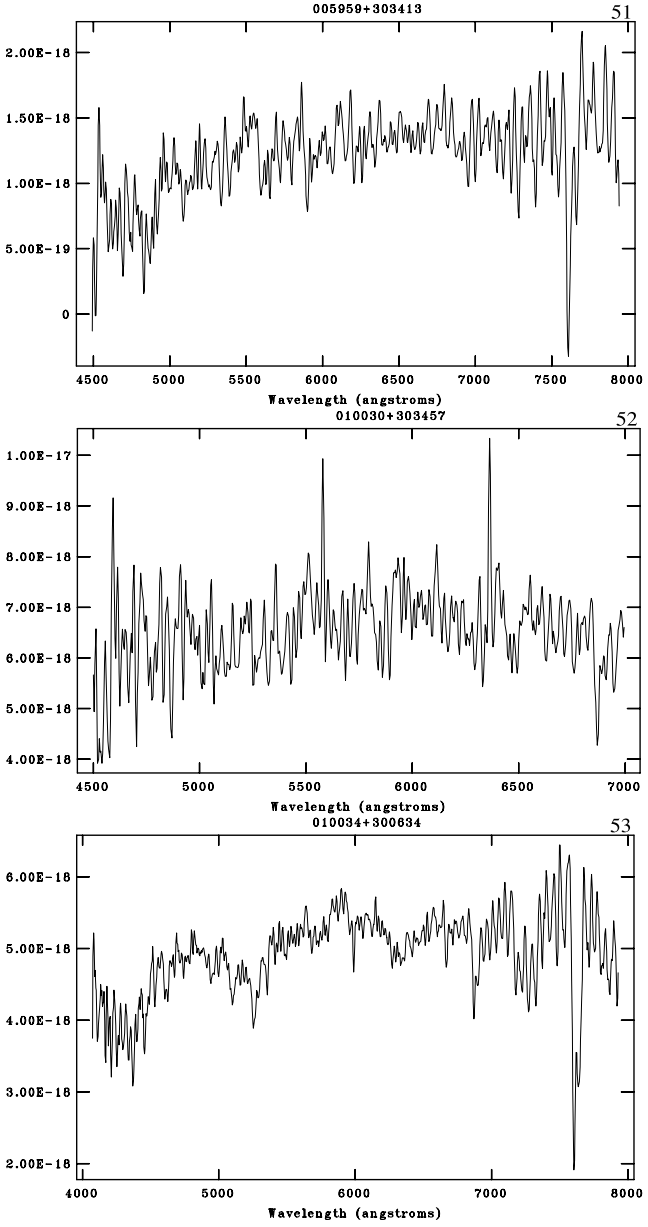

Figure A1 – *continued*

This paper has been typeset from a TEX/LATEX file prepared by the author.